Optical Multi-Mode Interference Devices Based on Self-Imaging: Principles and Applications

Lucas B. Soldano and Erik C. M. Pennings, *Member, IEEE*

Invited Paper

***Abstract*—This paper presents an overview of integrated optics routing and coupling devices based on multimode interference. The underlying self-imaging principle in multimode waveguides is described using a guided mode propagation analysis. Special issues concerning the design and operation of multimode interference devices are discussed, followed by a survey of reported applications. It is shown that multimode interference couplers offer superior performance, excellent tolerance to polarization and wavelength variations, and relaxed fabrication requirements when compared to alternatives such as directional couplers, adiabatic X- or Y-junctions, and diffractive star couplers.**

I. Introduction

TODAY'S evolving telecommunication networks are increasingly focusing on flexibility and reconfigurability, which requires enhanced functionality of photonic integrated circuits (PICs) for optical communications. In addition, modern wavelength demultiplexing (WDM) systems will require signal routing and coupling devices to have large optical bandwidth and to be polarization insensitive. Also small device dimensions and improved fabrication tolerances are required in order to reduce process costs and contribute to large-scale PIC production.

In recent years, there has been a growing interest in the application of multimode interference (MMI) effects in integrated optics. Optical devices based on MMI effects fulfil all of the above requirements, and their excellent properties and ease of fabrication have led to their rapid incorporation in more complex PICs such as phase diversity networks [1], Mach-Zehnder switches [2] and modulators [3], balanced coherent receivers [4], and ring lasers [5], [6].

This paper reviews the principles and properties of MMI devices and their applications. The operation of optical MMI devices is based on the self-imaging principle, presented in Section II. Basic properties of multimode waveguides are introduced early in Section III, followed by a short outline of the modal propagation analysis (MPA), which will be used later to describe image formation by general and restricted multimode interference (Sections IV and V, respectively). Special design and behavior issues concerning MMI devices are discussed in Section VI. Performances and compatibility with other components are presented through examples of fabricated MMI couplers and their applications in more elaborate optical circuits (Section VII). We conclude by comparing the properties of MMI devices with those of more conventional routing and coupling devices.

Manuscript received August 8, 1994; revised December 19, 1994. This work was supported in part by the Netherlands Technology Foundation (STW) as part of the programme of the Foundation for Fundamental Research on Matter (FOM).

L. B. Soldano is with Delft University of Technology, Department of Electrical Engineering, Laboratory of Telecommunication and Remote Sensing Technology, 2628 CD Delft, The Netherlands.

E. C. M. Pennings is with Philips Research Laboratories, Wideband Communication Systems, 5656 AA Eindhoven, The Netherlands.

IEEE Log Number 9409613.

II. The Self-Imaging Principle

Self-imaging of periodic objects illuminated by coherent light was first described more than 150 years ago [7]. Self-focusing (graded index) waveguides can also produce periodic real images of an object [8]. However, the possibility of achieving self-imaging in uniform index slab waveguides was first suggested by Bryngdahl [9] and explained in more detail by Ulrich [10], [11].

The principle can be stated as follows: *Self-imaging is a property of multimode waveguides by which an input field profile is reproduced in single or multiple images at periodic intervals along the propagation direction of the guide.*

III. Multimoded Waveguides

The central structure of an MMI device is a waveguide designed to support a large number of modes (typically $\geq$ 3). In order to launch light into and recover light from that multimode waveguide, a number of access (usually single-moded) waveguides are placed at its beginning and at its end. Such devices are generally referred to as $N \times M$ *MMI couplers*, where N and M are the number of input and output waveguides respectively.

A full-modal propagation analysis is probably the most comprehensive theoretical tool to describe self-imaging phenomena in multimode waveguides. It not only supplies the basis for numerical modelling and design, but it also provides insight into the mechanism of multimode interference. Other approaches make use of ray optics [12], hybrid methods [13], or BPM type simulations. We follow here the guided-mode propagation analysis (MPA), proposed first in [11] for the formulation of the periodic imaging.

Self-imaging may exist in three-dimensional multimode structures, for which MPA combined with two-dimensional (finite-element or finite-difference methods) cross-section calculations can provide a useful simulation tool [14]. However, the current trend of etch-patterning produces step-index waveguides, which are, in general, single-moded in the transverse direction. As the lateral dimensions are much larger than the transverse dimensions, it is justified to assume that the modes have the same transverse behavior everywhere in the waveguide. The problem can thus be analyzed using a two-dimensional (lateral and longitudinal) structure, such as the one depicted in Fig. 1, without losing generality. The analysis hereafter is based on such a 2-D representation of the multimode waveguide, which can be obtained from the actual 3-D physical multimode waveguide by several techniques, such as the effective index method (EIM) [15] or the spectral index method (SIM) [16].

A. Propagation Constants

Fig. 1 shows a step-index multimode waveguide of width W_M, ridge (effective) refractive index n_r and cladding (effective) refractive index n_c. The waveguide supports m lateral modes (as shown in Fig. 2) with mode numbers $\nu = 0, 1, \cdots (m-1)$ at a free-space wavelength λ_0. The lateral wavenumber $k_{y\nu}$ and the propagation constant β_ν are related to the ridge index n_r by the dispersion equation

$$k_{y\nu}^2 + \beta_\nu^2 = k_0^2 n_r^2 \tag{1}$$

with

$$k_0 = \frac{2\pi}{\lambda_0} \tag{2}$$

$$k_{y\nu} = \frac{(\nu+1)\pi}{W_{e\nu}} \tag{3}$$

where the "effective" width $W_{e\nu}$ takes into account the (polarization-dependent) lateral penetration depth of each mode field, associated with the Goos-Hähnchen shifts at the ridge boundaries. For high-contrast waveguides, the penetration depth is very small so that $W_{e\nu} \simeq W_M$. In general, the effective widths $W_{e\nu}$ can be approximated by the effective width W_{e0} corresponding to the fundamental mode [17], (which shall be noted W_e for simplicity):

$$W_{e\nu} \simeq W_e = W_M + \left(\frac{\lambda_0}{\pi}\right)\left(\frac{n_c}{n_r}\right)^{2\sigma}(n_r^2 - n_c^2)^{-(1/2)} \tag{4}$$

where $\sigma = 0$ for TE and $\sigma = 1$ for TM. By using the binomial expansion with $k_{y\nu}^2 \ll k_0^2 n_r^2$, the propagation constants β_ν can be deduced from (1)–(3)

$$\beta_\nu \simeq k_0 n_r - \frac{(\nu+1)^2 \pi \lambda_0}{4 n_r W_e^2}. \tag{5}$$

Therefore, the propagation constants in a step-index multimode waveguide show a nearly quadratic dependance with respect to the mode number ν.

By defining L_π as the beat length of the two lowest-order modes

$$L_\pi \doteq \frac{\pi}{\beta_0 - \beta_1} \simeq \frac{4 n_r W_e^2}{3\lambda_0} \tag{6}$$

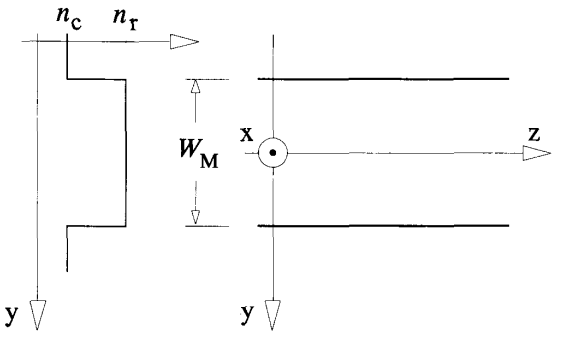

Fig. 1. Two-dimensional representation of a step-index multimode waveguide; (effective) index lateral profile (left), and top view of ridge boundaries and coordinate system (right).

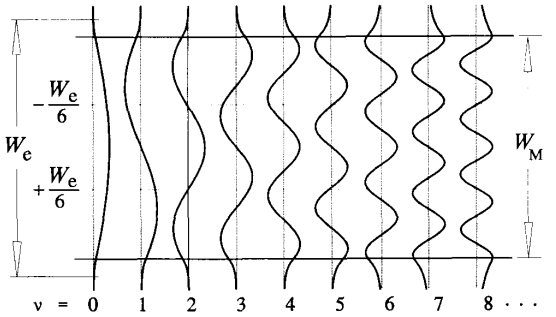

Fig. 2. Example of amplitude-normalized lateral field profiles $\psi_\nu(y)$, corresponding to the first 9 guided modes in a step-index multimode waveguide.

the propagation constants spacing can be written as

$$(\beta_0 - \beta_\nu) \simeq \frac{\nu(\nu+2)\pi}{3L_\pi}. \tag{7}$$

B. Guided-Mode Propagation Analysis

An input field profile $\Psi(y,0)$ imposed at $z = 0$ and totally contained within W_e (Fig. 3), will be decomposed into the modal field distributions $\psi_\nu(y)$ of *all* modes:

$$\Psi(y,0) = \sum_\nu c_\nu \psi_\nu(y) \tag{8}$$

where the summation should be understood as including guided as well as radiative modes. The field excitation coefficients c_ν can be estimated using overlap integrals

$$c_\nu = \frac{\int \Psi(y,0)\psi_\nu(y)\,dy}{\sqrt{\int \psi_\nu^2(y)\,dy}} \tag{9}$$

based on the field-orthogonality relations.

If the "spatial spectrum" of the input field $\Psi(y,0)$ is narrow enough not to excite unguided modes, (a condition satisfied for all practical applications), it may be decomposed into the

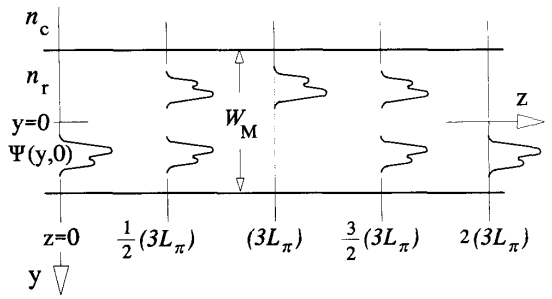

Fig. 3. Multimode waveguide showing the input field $\Psi(y,0)$, a mirrored single image at $(3L_\pi)$, a direct single image at $2(3L_\pi)$, and two-fold images at $\frac{1}{2}(3L_\pi)$ and $\frac{3}{2}(3L_\pi)$.

guided modes alone

$$\Psi(y,0) = \sum_{\nu=0}^{m-1} c_\nu \psi_\nu(y). \tag{10}$$

The field profile at a distance z can then be written as a superposition of all the guided mode field distributions

$$\Psi(y,z) = \sum_{\nu=0}^{m-1} c_\nu \psi_\nu(y) \exp[j(\omega t - \beta_\nu z)]. \tag{11}$$

Taking the phase of the fundamental mode as a common factor out of the sum, dropping it and assuming the time dependence $\exp(j\omega t)$ implicit hereafter, the field profile $\Psi(y,z)$ becomes

$$\Psi(y,z) = \sum_{\nu=0}^{m-1} c_\nu \psi_\nu(y) \exp[j(\beta_0 - \beta_\nu)z]. \tag{12}$$

A useful expression for the field at a distance $z = L$ is then found by substituting (7) into (12)

$$\Psi(y,L) = \sum_{\nu=0}^{m-1} c_\nu \psi_\nu(y) \exp\left[j\frac{\nu(\nu+2)\pi}{3L_\pi}L\right]. \tag{13}$$

The shape of $\Psi(y,L)$, and consequently the types of images formed, will be determined by the modal excitation c_ν, and the properties of the mode phase factor

$$\exp\left[j\frac{\nu(\nu+2)\pi}{3L_\pi}L\right]. \tag{14}$$

It will be seen that, under certain circumstances, the field $\Psi(y,L)$ will be a reproduction (self-imaging) of the input field $\Psi(y,0)$. We call *General Interference* to the self-imaging mechanisms which are independent of the modal excitation; and *Restricted Interference* to those which are obtained by exciting certain modes alone.

The following properties will prove useful in later derivations:

$$\nu(\nu+2) = \begin{cases} \text{even for } \nu \text{ even} \\ \text{odd for } \nu \text{ odd} \end{cases} \tag{15}$$

and,

$$\psi_\nu(-y) = \begin{cases} \psi_\nu(y) & \text{for } \nu \text{ even} \\ -\psi_\nu(y) & \text{for } \nu \text{ odd} \end{cases} \tag{16}$$

the latter being a consequence of the structural symmetry with respect to the plane $y = 0$.

IV. General Interference

This section investigates the interference mechanisms which are independent of the modal excitation, that is, we pose no restriction on the coefficients c_ν and explore the periodicity of (14).

A. Single Images

By inspecting (13), it can be seen that $\Psi(y,L)$ will be an image of $\Psi(y,0)$ if

$$\exp\left[j\frac{\nu(\nu+2)\pi}{3L_\pi}L\right] = 1 \quad \text{or} \quad (-1)^\nu. \tag{17}$$

The first condition means that the phase changes of all the modes along L must differ by integer multiples of 2π. In this case, all guided modes interfere with the same relative phases as in $z = 0$; the image is thus a *direct* replica of the input field. The second condition means that the phase changes must be alternatively even and odd multiples of π. In this case, the even modes will be in phase and the odd modes in antiphase. Because of the odd symmetry stated in (16), the interference produces an image *mirrored* with respect to the plane $y = 0$.

Taking into account (15), it is evident that the first and second condition of (17) will be fulfilled at

$$L = p(3L_\pi) \quad \text{with} \quad p = 0,1,2,\cdots \tag{18}$$

for p even and p odd, respectively. The factor p denotes the periodic nature of the imaging along the multimode waveguide. Direct and mirrored single images of the input field $\Psi(y,0)$ will therefore be formed by general interference at distances z that are, respectively, even and odd multiples of the length $(3L_\pi)$, as shown in Fig. 3. It should be clear at this point that the direct and mirrored single images can be exploited in bar- and cross-couplers, respectively.

Next, we investigate multiple imaging phenomena, which provide the basis for a broader range of MMI couplers.

B. Multiple Images

In addition to the *single* images at distances given by (18), *multiple* images can be found as well. Let us first consider the images obtained half-way between the direct and mirrored image positions, i.e., at distances

$$L = \frac{p}{2}(3L_\pi) \quad \text{with} \quad p = 1,3,5,\cdots. \tag{19}$$

The total field at these lengths is found by substituting (19) into (13)

$$\Psi\left(y, \frac{p}{2}3L_\pi\right) = \sum_{\nu=0}^{m-1} c_\nu \psi_\nu(y) \exp\left[j\nu(\nu+2)p\left(\frac{\pi}{2}\right)\right] \tag{20}$$

with p an odd integer. Taking into account the property of (15) and the mode field symmetry conditions of (16), (20) can be

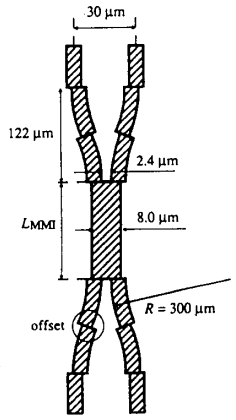

Fig. 4. Schematic layout of a 2 × 2 MMI coupler based on the general interference mechanism [19]. The multimode waveguide length is $L_{\mathrm{MMI}} \simeq 250\ \mu\mathrm{m}$. Offsets are used to minimize losses at the transitions between waveguides of different curvature. Note the widely spaced access branches, which decrease coupling between access waveguides and obviates blunting due to poor photolithography resolution.

written as

$$\Psi\left(y, \frac{p}{2}3L_\pi\right) = \sum_{\nu\ \mathrm{even}} c_\nu \psi_\nu(y) + \sum_{\nu \mathrm{odd}} (-j)^p c_\nu \psi_\nu(y) = \frac{1+(-j)^p}{2}\Psi(y,0) + \frac{1-(-j)^p}{2}\Psi(-y,0). \tag{21}$$

The last equation represents a pair of images of $\Psi(y,0)$, in quadrature and with amplitudes $1/\sqrt{2}$, at distances $z = \frac{1}{2}(3L_\pi)$, $\frac{3}{2}(3L_\pi)$, $\cdots$ as shown in Fig. 3. This two-fold imaging can be used to realize 2 × 2 3-dB couplers.

Optical 2 × 2 MMI couplers based on the single and two-fold imaging by general interference have been realized in III-V semiconductor waveguides [18], [19], in silica-based dielectric waveguides [20], and in non-lattice matched III-V quantum wells [21], [3].

Fig. 4 shows the schematic layout of the InGaAsP 2 × 2 multimode interference coupler reported in [18], [19]. The 8-μm wide multimode section supports 4 guided modes. Excess losses of 0.4–0.7 dB, with extinction ratios of −28 dB at the cross state ($3L_\pi = 500\ \mu$m) and imbalances well below 0.1 dB for the 3-dB state ($\frac{1}{2}3L_\pi = 250\ \mu$m) were measured for TE and TM polarizations at $\lambda_0 = 1.52\ \mu$m. The imbalance of an $N \times M$ coupler is defined as the maximum to minimum output power ratio for all M outputs, expressed in dB. This definition will be used throughout the paper.

In general, multi-fold images are formed at intermediate z-positions [12]. Analytical expressions for the positions and phases of the N-fold images have been obtained [22] by using Fourier analysis and properties of generalized Gaussian sums. A very brief summary of the bases and results of that derivation is given here. The starting point is to introduce a field $\Psi_{\mathrm{in}}(y)$ as the periodic extension of the input field $\Psi(y,0)$; antisymmetric with respect to the plane $y = 0$ (which, for this analysis, is chosen to coincide with one guide's lateral boundary), and with periodicity $2W_e$

$$\Psi_{\mathrm{in}}(y) \doteq \sum_{v=-\infty}^{\infty} [\Psi(y - v2W_e, 0) - \Psi(-y + v2W_e, 0)] \tag{22}$$

and to approximate the mode field amplitudes by sine-like functions

$$\psi_\nu(y) \simeq \sin(k_{y\nu} y). \tag{23}$$

Based on these considerations, (10) can be interpreted as a (spatial) Fourier expansion, and it is shown [22] that, at distances

$$L = \frac{p}{N}(3L_\pi) \tag{24}$$

where $p \geq 0$ and $N \geq 1$ are integers with no common divisor, the field will be of the form

$$\Psi(y, L) = \frac{1}{C}\sum_{q=0}^{N-1} \Psi_{\mathrm{in}}(y - y_q)\exp(j\varphi_q) \tag{25}$$

with

$$y_q = p(2q - N)\frac{W_e}{N} \tag{26}$$

$$\varphi_q = p(N - q)\frac{q\pi}{N} \tag{27}$$

where C is a complex normalization constant with $|C| = \sqrt{N}$, p indicates the imaging periodicity along z, and q refers to each of the N images along y.

The above equations show that, at distances $z = L, N$ images are formed of the *extended* field $\Psi_{\mathrm{in}}(y)$, located at the positions y_q, each with amplitude $1/\sqrt{N}$ and phase φ_q. This leads to N images (generally not equally spaced) of the *input* field $\Psi(y,0)$ being formed inside the physical guide (within the guide's lateral boundaries), as shown in Fig. 5. The multiple self-imaging mechanism allows for the realization of $N \times N$ or $N \times M$ optical couplers. Shortest devices are obtained for $p = 1$. In this case, the optical phases of the signals in a $N \times N$ MMI coupler are, (apart from a constant phase), given by

$$\varphi_{rs} = \frac{\pi}{4N}(s-1)(2N + r - s) + \pi \quad \text{for } r + s \text{ even} \tag{28}$$

and

$$\varphi_{rs} = \frac{\pi}{4N}(r + s - 1)(2N - r - s + 1) \quad \text{for } r + s \text{ odd} \tag{29}$$

where $r = 1, 2, \cdots N$ is the (bottom-up) numbering of the input waveguides and $s = 1, 2, \cdots N$ is the (top-down) numbering of the output waveguides.

It is important to note that the phase relationships given by (28) and (29) are inherent to the imaging properties of multimode waveguides. It appears that the output phases of the 4 × 4 coupler satisfy the phase quadrature relationship, and that this MMI device can be used as a 90°-hybrid which is a key component in phase-diversity or image rejection receivers and which can be used to avoid the quadrature problem in interferometric sensors.

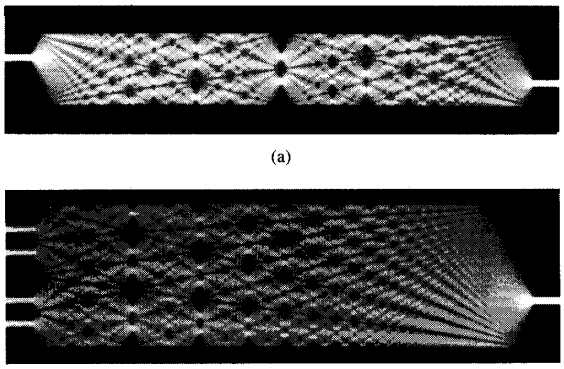

(a)

(b)

Fig. 5. Theoretical light intensity patterns corresponding to general or paired interference mechanisms in two multimode waveguides, leading to a mirrored single image (a), and a 4-fold image (b). Note also the multi-fold images at intermediate distances, non-equally spaced along the lateral axis. Reproduced by kind permission of J. M. Heaton, ©British Crown Copyright DRA 1992.

Several 4 × 4 MMI optical hybrids have been demonstrated in different technologies and sizes, such as 10–25 mm long semi-bulk constructions of sandwiched glass sheets [23], and ion-exchanged waveguides on glass substrates [24], [25].

Recently, ultra-compact (sub-millimeter length) 4 × 4 deeply etched waveguide couplers were fabricated by reactive-ion etching in III-V semiconductor material [26], [27]. These devices (shown in Fig. 6) attained excess losses below 1 dB, imbalances from 0.3–0.9 dB and phase deviations of the order of 5°.

V. Restricted Interference

Thus far, no restrictions have been placed on the modal excitation. This section investigates the possibilities and realizations of MMI couplers in which only some of the guided modes in the multimode waveguide are excited by the input field(s). This selective excitation reveals interesting multiplicities of $\nu(\nu+2)$, which allow new interference mechanisms through shorter periodicities of the mode phase factor of (14).

A. Paired Interference

By noting that

$$\mathrm{mod}_3[\nu(\nu+2)] = 0 \quad \text{for } \nu \neq 2, 5, 8, \cdots \tag{30}$$

it is clear that the length periodicity of the mode phase factor of (14) will be reduced three times if

$$c_\nu = 0 \quad \text{for } \nu = 2, 5, 8, \cdots \tag{31}$$

Therefore, as shown in [28], [29], single (direct and inverted) images of the input field $\Psi(y, 0)$ are now obtained at (cf. (18))

$$L = p(L_\pi) \quad \text{with} \quad p = 0, 1, 2, \cdots \tag{32}$$

provided that the modes $\nu = 2, 5, 8, \cdots$ are not excited in the multimode waveguide. By the same token, two-fold images are found at $(p/2)L_\pi$ with p odd. Based on numerical simulations,

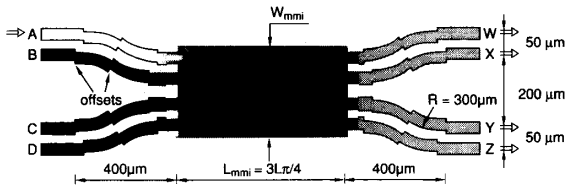

Fig. 6. Schematic layout of the 4 × 4 90°-hybrid and modal propagation analysis within the multimode waveguide [27]. The length and the width of the multimode waveguide are $L_{mmi} \simeq 945$ μm and $W_{mmi} \simeq 21.6$ μm, respectively.

N-fold images will be formed at distances (cf. (24))

$$L = \frac{p}{N}(L_\pi) \tag{33}$$

where $p \geq 0$ and $N \geq 1$ are integers having no common divisor.

One possible way of attaining the selective excitation of (31) is by launching an even symmetric input field $\Psi(y, 0)$ (for example, a Gaussian beam) at $y = \pm W_e/6$. At these positions, the modes $\nu = 2, 5, 8, \cdots$ present a zero with odd symmetry, as shown in Fig. 2. The overlap integrals of (9) between the (symmetric) input field and the (antisymmetric) mode fields will vanish and therefore $c_\nu = 0$ for $\nu = 2, 5, 8, \cdots$ Obviously, the number of input waveguides is in this case limited to two.

When the selective excitation of (31) is fulfilled, the modes contributing to the imaging are paired, i.e. the mode pairs 0-1, 3-4, 6-7, $\cdots$ have similar relative properties. (For example, each even mode leads its odd partner by a phase difference of $\pi/2$ at $z = L_\pi/2$—the 3-dB length—, by a phase difference of π at $z = L_\pi$—the cross-coupler length—, etc). This mechanism will be therefore called *paired* interference. Two-mode interference (TMI) can be regarded in this context as a particular case of paired interference.

2 × 2 MMI couplers based on the paired interference mechanism have been demonstrated in silica-based dielectric rib-type waveguides with multimode section lengths of 240 μm (cross state) and 150 μm (3-dB state) [30], [31]. Insertion loss lower than 0.4 dB, imbalance below 0.2 dB, extinction ratio of −18 dB, and polarization-sensitivity loss penalty of 0.2 dB were reported for structures supporting 7–9 modes. Calculations predict that power excitation coefficients as low as −40 dB for the modes $\nu = 2, 5, 8$ can be achieved through a correct positioning of the access waveguides, remaining below −30 dB for a 0.1-μm misalignment [29].

Recently, extremely small paired-interference MMI devices were reported [32]. The 3-dB (cross) couplers, realized in a raised-strip InP-based waveguide, are 107-μm (216-μm) long, and show 0.9-dB (2-dB) excess loss and −28 dB crosstalk.

B. Symmetric Interference

Optical N-way splitters can in principle be realized on the basis of the general N-fold imaging at lengths given by (24). However, by exciting only the even symmetric modes, 1-to-N beam splitters can be realized with multimode waveguides four times shorter [33].

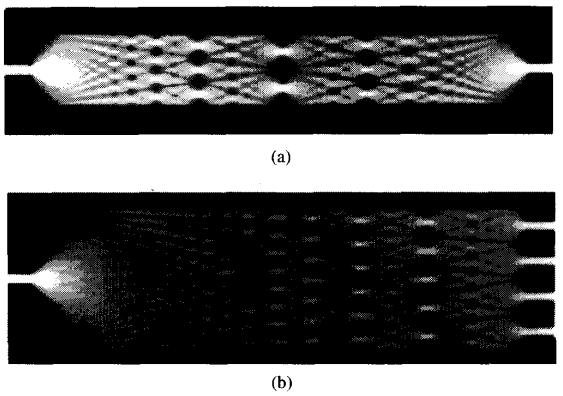

Fig. 7. Theoretical light intensity patterns corresponding to (single-input) symmetric interference mechanisms in a 20-μm-wide multimode waveguide, showing "1 × 1" imaging (a); and in a 40-μm-wide multimode waveguide, showing 1-to-4 way splitting (b). Note also the multi-fold images at intermediate distances, equally spaced along the lateral axis. Reproduced by kind permission of J. M. Heaton *et al.* [34]. ©British Crown Copyright DRA 1992.

In effect, by noting that

$$\mathrm{mod}_4[\nu(\nu+2)] = 0 \quad \text{for } \nu \text{ even} \tag{34}$$

it is clear that the length periodicity of the mode phase of (14) will be reduced four times if

$$c_\nu = 0 \quad \text{for } \nu = 1, 3, 5, \cdots \tag{35}$$

Therefore, single images of the input field $\Psi(y, 0)$ will now be obtained at (cf. (18))

$$L = p\left(\frac{3L_\pi}{4}\right) \quad \text{with } p = 0, 1, 2, \cdots \tag{36}$$

if the odd modes are not excited in the multimode waveguide. This condition can be achieved by centre-feeding the multimode waveguide with a symmetric field profile. The imaging is obtained by linear combinations of the (even) symmetric modes, and the mechanism will be called *symmetric* interference.

In general, N-fold images are obtained [33], [34] at distances (cf. (24))

$$L = \frac{p}{N}\left(\frac{3L_\pi}{4}\right) \tag{37}$$

with N images of the input field $\Psi(y, 0)$, symmetrically located along the y-axis with equal spacings W_e/N.

Fig. 7 shows the calculated intensity patterns inside the multimode waveguide of single-input, symmetrically excited MMI couplers [34]. At mid-way from the self-imaging length, a two-fold image is formed. The number of images increases at even shorter distances, according to (37), until they are no longer resolvable. A good rule of thumb is that in order to obtain low-loss well-balanced 1-to-N splitting of a Gaussian field, the multimode waveguide is required to support at least $m = N + 1$ modes [35].

The 1 × 2 waveguide splitter/combiner is perhaps the simplest MMI structure ever realized, needing just two symmetric modes. Extremely short splitters (20–30 μm for silica-based and 50–70 μm for InP-based waveguides) have been fabricated with excess losses of around 1 dB and imbalances below 0.15 dB [36], in agreement with numerical predictions [37], [38].

TABLE I
SUMMARY OF CHARACTERISTICS OF THE GENERAL, PAIRED, AND SYMMETRIC INTERFERENCE MECHANSIMS

Interference mechanism	*General*	*Paired*	*Symmetric*
Inputs × Outputs	$N \times N$	$2 \times N$	$1 \times N$
First single image distance	$(3\ L_\pi)$	(L_π)	$(3\ L_\pi)/4$
First N-fold image distance	$(3\ L_\pi)/N$	$(L_\pi)/N$	$(3\ L_\pi)/4\ N$
Excitation requirements	none	$c_\nu = 0$ for $\nu = 2, 5, 8 \ldots$	$c_\nu = 0$ for $\nu = 1, 3, 5 \ldots$
Input(s) location(s)	any	$y = \pm W_e/6$	$y = 0$

A number of $1 \times N$ waveguide splitters/combiners covering a wide range of different multimode guide widths (12–48 μm) and lengths (250–3800 μm) have been demonstrated in GaAs- and InP-based rib waveguides which divide power with <0.4-dB imbalances between N output guides, for values of N between 2 and 20 [34], [39], [40].

These experiments permit to conclude that, setting 1 μm as an achievable lithographic limit to the open gap, and 2 μm as a workable width of the access waveguides, InP-based 1-to-N way splitters at $\lambda_0 = 1.55$ μm could be as short as $N \times 20$ μm.

VI. Discussion

MMI devices differ from other routing and coupling devices in a number of aspects. This section discusses how self-imaging determines design and behavior characteristics of MMI devices in comparison to alternative devices.

Table I summarizes some characteristics of the general, paired and symmetric interference mechanisms.

A. Properties and Requirements

The general interference mechanism is in principle independent of the position and shape of the input fields. However, MPA calculations and experiments for strongly-guiding structures [26], and full 3-D calculations for weakly- as well as strongly-guiding structures [14], have shown that the performance of MMI devices based on general interference can be further optimized by careful positioning of the access waveguides.

Restricted (paired and symmetric) interference mechanisms must have well-located and reasonably symmetric input field(s) in order to comply with the selective modal excitation requirements of (31) and (35), respectively.

For the case of 2 × 2 couplers, paired interference actually leads to longer devices than those based on the general interference mechanism. The selective excitation requirement dictates an increase in the multimode waveguide width—and therefore in its length (see (6))—which cancels out the potential length reduction. However, general interference mechanisms in weakly guiding structures may suffer from higher losses than paired interference, due to decreased image resolution (Section 6.2). The access waveguides positioned at the corners of the multimode waveguide (Fig. 4) cause the image to be reconstructed mainly by the (wider) outer lobes of the high-order modes (see [14]).

B. Imaging Quality

Imaging quality refers to how accurately the input field is reproduced at the end of the multimode waveguide.

The quadratic dependence of the propagation constants with the mode number, found in (5), is an approximation. This means that the guided modes will actually accumulate small deviations from the calculated phases at the imaging distances, which tend to blur the reconstructed image field. This situation is analogous to the focal shift from paraxial rays prediction due to aberration in optical systems of finite aperture. However, some balancing of the phase errors—and thus an improvement of the imaging quality—is possible by a slight correction of the imaging lengths predicted by (24), (33), and (37), [35].

The imaging quality of a multimode waveguide can be formally evaluated with its line-spread function (LSF) [35]. The LSF represents the complex image field of an infinitely narrow input field. An imaging system of high resolution and good contrast is characterized by a narrow-peak and low-ripple LSF.

In device terms, a narrow-peak and low-ripple LSF means low insertion loss and low crosstalk, respectively. The characteristics of the LSF are given by the discrete modal amplitude spectrum c_ν from (9). A flat mode amplitude spectrum (i.e., all guided modes equally excited) with a sharp cut-off will produce a maximally narrow but heavily rippled LSF. Conversely, a ripple-free but broader LSF can be obtained by a smooth roll-off in the mode spectrum (i.e., gradually decreasing excitation coefficients for the higher-order modes).

A simple way of estimating the imaging resolution of a multimode waveguide is as follows. As the image field is a linear combination of the guided mode fields, the narrowest obtainable image in a multimode waveguide, and thus its resolution ρ, will be roughly equal to the cosine-like lobe width of the highest supported mode (i.e., its spatial half-period, see Fig. 2)

$$\rho \simeq \frac{W_e}{m}. \tag{38}$$

A much more elaborate analysis, involving the calculation of the LSF [35], predicts a resolution ranging from 0.89 W_e/m (for a flat mode spectrum) to approximately 1.50 W_e/m (for a Gaussian mode spectrum). Practical MMI devices usually have smoothly decaying mode spectra.

The imaging resolution is a useful parameter in designing an MMI coupler. The multimode waveguide must be able to provide an image field as narrow as the input field(s) launched from the access waveguide(s). For a given width of the multimode waveguide, the resolution ρ is determined by the number of guided modes m. The number of guided modes, in turn, is determined by the lateral refractive index contrast in ridge (rib) waveguides, whereas it is determined by the transversal contrast in deeply etched (raised-strip) waveguides.

C. Loss, Balance, and Phases

Employing MMI effects can produce low-loss devices, due to the efficient imaging of the input of the MMI section onto the output. In addition, an increased guide-separation prevents coupling between the access guides and leads to a sharp onset of coupling in the MMI section. This prevents additional, difficult to control, power exchange in the access guides and associated radiation losses, a problem commonly found in directional couplers.

For many applications, balancing is even more important than the insertion loss. In coherent detection techniques for example, the balancing of the output powers of the 3-dB coupler determines the suppression of the RIN noise of the local oscillator laser. And when 3-dB couplers are used in Mach-Zehnder modulators or switches, the balancing directly translates into extinction ratio and crosstalk. With respect to balancing, MMI devices operate fundamentally different from directional couplers. The output powers of a directional coupler are proportional to $\cos^2(\pi z/2L_\pi)$ and $\sin^2(\pi z/2L_\pi)$, meaning that the sensitivity of the transmission to length variations is maximum at the 3-dB point and of opposite sign for each output. MMI-devices function differently as can be seen in Fig. 8 which shows the simulated behavior of the 4 $\times$ 4 90°-hybrid reported in [27]. Each single image of the 4-fold image is a local maximum, implying that the sensitivity is minimum at the optimum length of $L = 978$ μm and that all output powers *decrease similarly* for deviations from the optimum length. As a consequence, balancing remains better than 0.3 dB for a total range of $L = 978 \pm 25$ μm, leading to common mode rejection ratios in excess of 30 dB for the entire 50 μm range.

Since the output phases of the 90°-hybrid (see (27)) are inherently linked to the 4-fold image, the output phases remain within a margin of $\pm$ 5°from the phase quadrature relationship for the same 50 μm range. The excellent balancing and the stable phase relationships, in turn lead to a total 40 μm range where the simulated image rejection ratio is better than 30 dB. This analysis is not specific for the 4 $\times$ 4 hybrid, but holds for MMI devices in general which has been confirmed by several experimental observations [19], [27], [41].

D. Reflections Properties

Several applications such as lasers and coherent detection techniques are very sensitive to reflections. Reflections in MMI devices may originate at the end of the MMI-section in between the output guides. Nonnegligible reflections may occur when large refractive index differences are encountered such as the semiconductor-air interface in deeply etched waveguides. For *nonoptimum* lengths, some light may be reflected off the end of the MMI section and may eventually reach the input guides. However, even for *optimum* lengths, reflections in MMI devices can be surprisingly effective, because the reflection mechanisms involve the very same imaging property of multimode waveguides. Two different reflection mechanisms have been identified [44]:

1) An "internal resonance" mechanism, which is caused by the presence of several *simultaneously* occurring self-images. For example, the MMI 3-dB coupler shown in Fig. 4 is based on the two-fold image occurring at a length of $L = 3L_\pi/2$ as given by (19). This length equals precisely twice the self-imaging length for symmetric excitation $L = 3L_\pi/4$ as given

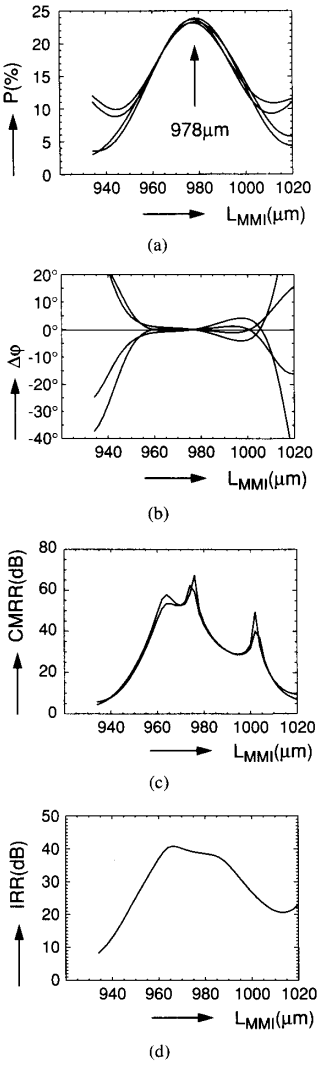

Fig. 8. Simulated performance for 4 × 4 90°-hybrid: (a) relative output power, (b) phase deviation from the phase quadrature condition, (c) common mode rejection ratio, and (d) image rejection ratio.

by (36). This symmetric self-imaging mechanism ensures efficient imaging of both reflecting ends onto each other as illustrated in Fig. 9. In lasers employing such an MMI 3-dB coupler, this "internal resonance" may show up as a separate contribution in the laser spectrum [45]. Simultaneously occurring general and symmetric self-imaging mechanisms can possibly be prevented by employing couplers based on the paired interference mechanism.

2) A second type of reflection is encountered when an MMI power splitter is used in reverse as a power combiner. Efficient combining operation requires inputs of equal amplitude and phase. If, however, the two inputs are 180° out of phase, power is minimum in the output guide but maximum at the reflecting end of the MMI section. This leads to perfect imaging of the input guides back onto themselves. Back reflection can thus

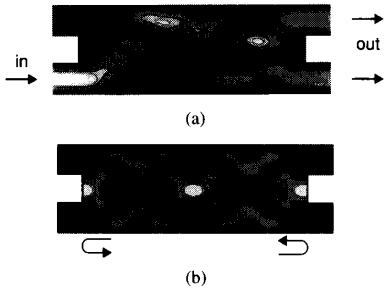

Fig. 9. MPA-simulated field contour plots in a general-interference 2 × 2 3-dB MMI coupler: (a) transmission and (b) internal resonance.

vary from a minimum for in-phase excitation to a maximum for out-of-phase excitation for a single MMI combiner optimized for maximum transmission. Note that this reflection mechanism can cause increased back reflection during the off-state of a Mach-Zehnder modulator using a 2 × 1 MMI combining element. This potential type of reflection can be avoided by using a Mach-Zehnder switch incorporating a 2 × 2 3-dB coupler rather than a combiner.

For reflection-sensitive applications, several means can be used to achieve an effective reduction of reflections, such as using low-contrast waveguides or tapering the ends of the MMI section [44].

E. Tolerances

Relaxed tolerances are important for fabrication as well as for operating conditions. Fabrication tolerances refer to the control of the geometrical dimensions during processing and its subsequent impact on device performance. Operation tolerances relate to the device behavior for changes in the wavelength, polarization, temperature, input field distribution, and refractive index.

A tolerance analysis can be performed [46] in which each image is considered as a Gaussian beam focused at a self-image distance $z = L$. Then, the loss penalty produced by a (small) finite shift δL in the z-position of the output waveguides can be evaluated by overlapping the defocused beam with the output waveguide mode field. It is found that the length shift which produces a 0.5-dB loss penalty is approximately equal to the so-called Rayleigh range:

$$\delta L \simeq \frac{\pi n_r w_0^2}{4\lambda_0} \tag{39}$$

where w_0 is defined here as the Gaussian beam waist, and equals the full $1/e$ amplitude width of the input field $\Psi(y, 0)$. Equation (39) can be interpreted as an absolute length tolerance, which does not depend on the dimensions of the multimode waveguide. An important conclusion is that, for a given wavelength and technology, all tolerances can be relaxed by using wider access waveguides. Tapered access waveguides have been successfully experimented in deeply-etched InP-based MMI couplers, resulting in a tolerant process and low-loss operation [42].

The tolerances corresponding to other fabrication or operation parameters can now be related to δL from (18), using

TABLE II
DESIGN PARAMETERS OF MMI DEVICES FABRICATED IN III-V SEMICONDUCTOR MATERIALS, AND EXPERIMENTALLY MEASURED TOLERANCE FIGURES FOR A GIVEN LOSS PENALTY. PARENTHESIZED NUMBERS ARE RESULTS OF NUMERICAL SIMULATIONS BY MPA OR BPM

Interference mechanism	$N \times M$	*Ref.*	n_r	λ_0 [μm]	w_0 [μm]	W_M [μm]	L [μm]	*Loss penalty* [dB]	*Imbalance* [dB]	δW_M [μm]	$2\delta\lambda_0$ [nm]
General	2×2	[19]	3.24	1.52	3.0	8.0	240	(0.8)	(0.17)	(0.20)	(100)
	2×2	[42]	3.28	1.51	3.0	7.5	250	0.5	0.1	0.20	
	4×4	[27]	3.24	1.52	3.0	21.6	945	(2.0)		(0.20)	
Paired	2×2	[41]	3.29	1.53	3.0	18.0	530	0.5	0.20	0.30	100
	2×2	[43]	3.30	1.51	2.2	16.0	425	0.5	0.20	0.25	
Symmetric	1×4	[34]	3.47	1.06	2.6	40.0	1300			(0.25)	
	1×4	[40]	3.30	1.55	2.5	24.0	300	0.4	0.20	0.30	(60)

the definition of (6)

$$\frac{\delta L}{L} = 2\frac{\delta W_e}{W_e} \simeq \frac{|\delta\lambda_0|}{\lambda_0} \simeq \frac{\delta n_r}{n_r}. \tag{40}$$

Hence, it is apparent that the multimode waveguide length L must be made as short as possible in order to allow for relaxed tolerances to the other parameters.

As an example, let us consider the 2 × 2 MMI coupler of Fig. 4 [19], comprising a multimode waveguide with $W_e \simeq 8$ μm, $L = 240$ μm and $n_r = 3.24$, fed by access waveguides with $w_0 \simeq 3$ μm, and operated at 1.52-μm wavelength. From (39), $\delta L \simeq 15$ μm; which substituted into (40) yields $\delta W_e \simeq 0.25$ μm, $\delta\lambda \simeq 95$ nm, and $\delta n_r \simeq 0.20$. Thus, the multimode section width is by far the most critical parameter to control during fabrication. In a development stage, small variations in the width can be compensated for by varying lengths in steps of δL. In our example, five lengths $L = 220$, 235, 250, 265, and 280 μm are sufficient to obtain at least a pair of devices performing very close to design values. Table II summarizes reported tolerance figures of MMI devices, for specified penalty losses and imbalances.

The dependence on polarization changes, which may be investigated through the term $(n_r W_e^2)$ in (6), results in slightly different optimum imaging lengths for both polarizations. Polarization-independent operation is then possible by designing at an intermediate length, at the price of a small loss increase. Polarization-change induced penalty losses below 0.30 dB have been calculated and experimentally verified in 2 × 2 strip-loaded waveguide MMI couplers [41].

VII. APPLICATIONS

In addition to their use as single routers or couplers, MMI devices have been applied to perform a number of more complex functions. Soon after the theory of the self-imaging principle in multimode waveguides was established [10], [35], an MMI modulator or switch in $LiNbO_3$ was demonstrated, which achieved 0.5-dB loss and 13–20 dB extinction ratios by a nonuniform electro-optical modulation of the refractive index profile in the multimode waveguide [47], [47], thus effectively combining the coupling and the phase shift functions in one single device.

Further applications concentrated more on making use of MMI couplers as constituents of larger passive and/or active structures. The following examples illustrate their compatibility to many types of materials and technologies, and highlight how their performances are used to an advantage in OEICs.

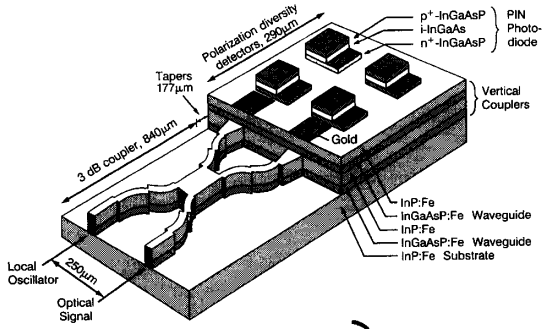

Fig. 10. Schematic of polarization-diversity balanced coherent receiver front-end OEIC [4].

A. Coherent Receiver Front-End

Possibly the earliest reported application using an MMI device in a complex photonic integrated circuit is the coherent receiver front-end [4], [49], [50] shown in Fig. 10. This chip contains an MMI 3-dB coupler to combine the optical powers from the photosignal and the local oscillator laser. In addition, two pairs of polarization-sensitive photodetectors generate a polarization-insensitive IF signal using diversity architectures. Several key features of MMI devices enhanced the overall performance of the chip.

The ultracompact size of the MMI 3-dB coupler (298 μm) and its compatibility with deeply etched waveguides allowing for monomode ultracompact bends ($R = 250$ μm), led to a total chip size of merely 1.3 mm.

Balanced operation is important to fully use the available optical powers of the photosignal and the LO laser and to minimize common mode noise due to LO intensity fluctuations. Typical measured balance of both coupler outputs was within ±0.11 dB for both polarizations leading to measured common mode rejection ratios of 32 dB and better [4].

The polarization insensitive behavior of the MMI 3-dB coupler is crucial since polarization splitting is achieved after the 3-dB coupler by means of polarization selective photodetector pairs. This configuration has the advantage, that in addition to being suitable for polarization-diversity reception, it is also suitable for phase-diversity detection, which has been tested in a 2.5 Gbit/s phase-diversity homodyne detection experiment [50], [51].

The wavelength insensitive behavior of the 3-dB coupler in combination with the compact design of the photodetectors

should result in a broad spectral operating range (≈70 nm) [19], [52].

B. Mach-Zehnder Structures

Mach-Zehnder interferometers have been extensively used in practical realizations of optical processing because of their natural physical separation between the splitting/recombining functions and the phase-shifting function.

The extinction ratio in a Mach-Zehnder interferometer is directly limited by the imbalance of the input splitter and the output combiner. For example, a 0.2-dB power imbalance would limit the extinction ratio to −33 dB. In addition, an output phase deviation of the splitting/combining elements will further worsen the extinction ratio in passive interferometers or (in the case of an active device) will have to be compensated for by forcing a biasing phase-shift driving voltage.

The good balancing and stable relative phases shown by MMI couplers around their optimum operating point (see Section VI-C), together with their polarization insensitivity make these devices ideal candidates for integration into Mach-Zehnder structures.

A passive polarization splitter comprising a pair of 3-dB MMI couplers in a Mach-Zehnder structure provided TE (TM) extinction ratios better than −16 dB (−13 dB) over a 60-nm wavelength range [43]. Electro-optic Mach-Zehnder interferometer switches including 3-dB MMI couplers have been demonstrated in double-heterostructure (DH) [2] as well as multi-quantum wells (MQW) [3], [53] III-V materials, featuring extinction ratios ranging from −10 dB to −19 dB. Mach-Zehnder interferometers with MMI splitters and recombiners have also been experimented in hollow dielectric waveguides operated at 10.6-μm wavelength [54].

In all these designs, MMI couplers played a crucial role in attaining large bandwidth and polarization independent operation.

The possibility of achieving $1 \times N$ and $N \times N$ splitter/combiners with MMI devices allows the realization of very compact integrated multiway optical switches. Such a function is performed in a so-called multi-arm or generalized Mach-Zehnder interferometers [55] (shown in Fig. 11), where the input signal is split by a $1 \times N$ (or $N \times N$) MMI splitter, fed into individually addressable waveguide phase shifters, and recombined in an $N \times N$ MMI coupler. By controlling N phase shifters, the input signal(s) can be made to switch to any one (or certain sets) of the N output waveguides, though not independently [55], [56]. Multiway switches have been demonstrated in generalized Mach-Zehnder structures incorporating MMI splitters and combiners. The 1×10 (10.6-mm long) and 10×10 (13.1-mm long) switches in GaAs/AlGaAs [56] showed ±9% switching uniformity, −10 dB maximum crosstalk, and around 6-dB excess loss. A 1×4 switch in InGaAsP/InP achieved −13 dB crosstalk and polarization insensitivity [57].

C. Ring Lasers

MMI devices have also proven to be successful outcoupling elements in ring lasers. The outcoupling element has a crucial influence on the performance of the ring laser, since the outcoupler forms an integral part of the ring resonator [58]. The most commonly used outcoupling element is the Y-junction, which offers ease of design, but can only couple one of the counter-propagating beams out of the ring. Directional couplers have not proven to be a successful outcoupler, partly due to their incompatibility with high-contrast waveguides which are required to create low-loss small-radii bends. MMI devices on the other hand provide symmetric outcoupling, relaxed fabrication tolerances, ease of design and compatibility with high-contrast waveguides.

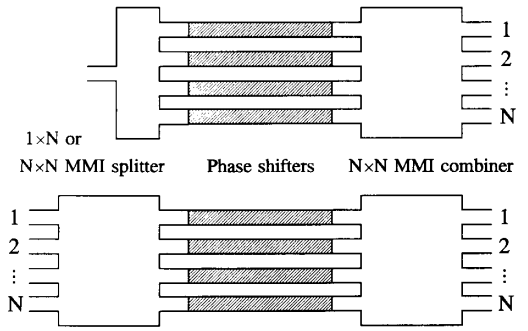

Fig. 11. Schematic layouts of a $1 \times N$ and an $N \times N$ generalized Mach-Zehnder interferometers, comprising MMI couplers as splitting/combining elements, and waveguide phase shifters.

The first ring lasers using MMI 3-dB outcouplers ($L = 233$ μm) were reported for $\lambda_0 \approx 1.6$ μm in GaInAsP/InP using deeply etched waveguides thereby enabling low-loss $R = 150$ μm bends [5], [6]. A differential quantum efficiency of $\eta_{\text{ext}} = 3.9\%$ was reported with almost kink-free LI curves at CW operation and at 20°C [6]. An additional MMI combiner has been used to combine both counter-propagating beams in a single output waveguide, thereby increasing the efficiency to $\eta_{\text{ext}} = 5.2\%$ [6]. Stable single-mode operation has been observed with a sidemode suppression of 35 dB. Occasional mode-hopping and stable single mode operation have been explained as being due to coupled cavity behavior caused by reflections in the output path and in the MMI devices (see Section 6.4 and [44]).

MMI 3-dB couplers have also been incorporated in GaAs/AlGaAs ring lasers using low-contrast waveguides ($R = 400$ μm), with a reported differential quantum efficiency of $\eta_{\text{ext}} = 7\%$ at $\lambda_0 \approx 0.87$ μm and for CW operation [59]. In these experiments, the compatibility of MMI couplers with low-contrast waveguides was successfully demonstrated.

Comparing the performance of ring lasers employing MMI couplers to those using Y-junctions [6], [60] or directional couplers [60], the stability of the splitting ratio of the outcoupler is found to be the key factor. Lasers are subject to varying operating conditions; changes in current affect the gain spectrum, change the temperature and cause carrier induced refractive index changes. If the splitting ratio of the outcoupler, in turn, depends on wavelength, refractive index or excitation conditions, unstable lasing operation results, since laser performance is determined by the interplay of all these parameters. It is therefore the extreme stability of the splitting

TABLE III
REPRESENTATIVE CHARACTERISTICS AND EXPERIMENTALLY MEASURED PERFORMANCES OF INTEGRATED OPTICAL ROUTERS AND COUPLERS. PARENTHESIZED NUMBERS ARE RESULTS OF NUMERICAL SIMULATIONS BY MPA OR BPM

Device type	*Ref.*	*Inputs × outputs*	*Material*	*Excess loss* [dB]	*Imbalance* [dB]	*Bandwidth* [nm]	*Polarization penalty* [dB]	*Size*
Y-junction	[63]	1×2	GaAs/GaAlAs	2.0–6.0	0.1–0.5	large	low	< 6°
X-junction	[64]	2×2	$LiNbO_3$	<1.0	>20	large	low	> 6°
Parallel coupler	[65]	2×2	Silica	0.1–0.2	0.6	200	0.3	4 mm
TMI coupler	[66]	2×2	InGaAsP/InP	1.0–3.0	0.1	15		400 μm
MMI coupler	[19]	2×2	InGaAsP/InP	0.1–0.3	<0.05	(100)	0.2	240 μm
MMI coupler	[41]	2×2	InGaAsP/InP	0.3–0.6	<0.1	80–100	0.3	530 μm
Tree-coupler	[67]	1×16	InGaAsP/InP	2.0–3.0	2.6–4.0		<1.0	~1 mm
MMI splitter	[34]	1×2 ... 20	GaAs/AlGaAs	~0	0.35			N×120 μm
MMI splitter	[39]	1×4	InGaAsP/InP	0.1	0.1	(60)		300 μm
MMI splitter	[42]	1×16	InGaAsP/InP	2.2	1.5		0.4	140 μm
Star-coupler	[68]	19×19	Silica	1.5	2.0			7.5 mm
Star-coupler	[69]	8×8	Silica	1.4–1.7	1.3–1.5	200	0.3	1.5 mm
MMI coupler	[26]	4×4	InGaAsP/InP	1.0	0.3–0.9		0.2	945 μm
MMI coupler	[56]	10×10	GaAs/AlGaAs	≤3.0	0.1–0.2			3270 μm

ratio of the MMI coupler, as discussed in Section 6.3, that leads to the improved performance of ring lasers incorporating MMI couplers.

VIII. CONCLUSION

In this paper, we have reviewed integrated optical devices based on multimode interference. The theory behind the self-imaging principle was outlined in order to show the versatility of multimode interference. MMI devices are capable of providing a wide range of $N \times M$ coupling functions, with insertion losses below 0.5 dB, crosstalk figures as low as -30 dB and balancing within 0.2 dB. These features, together with their tolerance to process and operation parameters, have led to the rapid incorporation of MMI devices in balanced receivers, Mach-Zehnder structures and ring lasers.

MMI devices have emerged as a new class of components which can provide coupling and splitting from/into a number of channels, with low loss and good balancing. As such, they might be compared to more conventional devices performing similar functions, such as directional couplers, adiabatic elements (X- or Y-junctions), diffractive structures (tree- or star-couplers), and two-mode interference (TMI) couplers. Table III summarizes important characteristics of coupling and routing devices. The table provides an overview of experimental performances, and is intended for a general comparison between traditional components and MMI devices. However, it should be used with care; the reported works encompass a number of different materials and wavelengths.

In addition to the figures presented in Table III, some other (non quantifiable) advantages of MMI devices are worth mentioning. In the first place, the design procedure can be performed quite easily; all is needed is to calculate first the beat length L_π with (6) and then to obtain the imaging length with Table I for the chosen structure. Secondly, cascadeability is not an issue; it is possible to obtain well-balanced 1-to-N splitting with just one single MMI device, albeit at the expense of an optical bandwidth penalty. Thirdly, MMI structures are compatible with both weakly guiding waveguides as well as with deeply etched waveguides, and are almost completely independent of the transverse structure.

Novel structures and applications are currently being investigated, with promising results. Symmetric-interference 1 × 1 may be useful for filtering out the unwanted lowest-order antisymmetric mode of an input guide, while linearly tapered 1 × 1 or 1 × 2 MMI power splitters can act as field transformers in transitions between waveguides of different width [61]. Very recently, restricted-interference mechanisms were found which perform certain non-uniform (e.g. 28/72 or 15/85) splitting functions in 2 × 2 couplers. Based on this, MMI couplers with up-down tapered multimode sections were demonstrated which allow to freely choose the splitting ratios within a few percents [62], thus opening the way for these devices to perform "tap" functions in communication networks, and allowing more freedom in the design of ring lasers.

Considering the records of MMI devices so far, both as single couplers capable of enhancing the performance of larger photonic circuits or as new components allowing new functionalities, we foresee an increasing exploitation of the self-imaging principle in integrated optics.

ACKNOWLEDGMENT

The authors wish to acknowledge fruitful discussions and material contributed to this paper by J. M. Heaton of Defence Research Agency; R. J. Deri of Lawrence Livermore National Laboratory; B. H. Verbeek of Philips Optoelectronics Center; M. K. Smit of Delft University of Technology; and M. Bachmann, and P. A. Besse of the Swiss Federal Institute of Technology.

REFERENCES

[1] L. B. Soldano, M. K. Smit, A. H. de Vreede, J. W. M. van Uffelen, B. H. Verbeek, P. van Bennekom, W. H. C. de Krom, and W. van Etten, "New all-passive 4 × 4 planar optical phase diversity network," in *Proc. European Conf. Opt. Commun. (ECOC)*, Paris, France, Sept. 1991, pp. 96–99.

[2] M. Bachmann, M. K. Smit, L. B. Soldano, P. A. Besse, E. Gini, and H. Melchior, "Polarization-insensitive low-voltage optical waveguide switch using InGaAsP/InP four-port Mach-Zehnder interferometer," in *Proc. Conf. Opt. Fiber Commun. (OFC)*, San Jośe, CA, 1993, pp. 32–33.

[3] J. E. Zucker, K. L. Jones, T. H. Chiu, and K. Brown-Goebeler, "Strained quantum wells for polarization-independent electroopic wave-

guide switches," *J. Lightwave Technol.*, vol. 10, no. 12, pp. 1926–1930, 1992.
[4] R. J. Deri, E. C. M. Pennings, A. Scherer, A. S. Gozdz, C. Caneau, N. C. Andreadakis, V. Shah, L. Curtis, R. J. Hawkins, J. B. D. Soole, and J. I. Song, "Ultracompact monolithic integration of balanced, polarization diversity photodetectors for coherent lightwave receivers," *IEEE Photon. Technol. Lett.*, vol. 4, no. 11, pp. 1238–1240, 1992.
[5] M. J. N. van Stralen, R. van Roijen, E. C. M. Pennings, J. M. M. van der Heijden, T. van Dongen, and B. H. Verbeek, "Design and fabrication of integrated InGaAsP ring lasers with MMI-outcouplers," in *Proc. European Conf. Integrated Optics (ECIO)*, Neuchâtel, Switzerland, Apr. 1993, pp. 2.24–2.25.
[6] R. van Roijen, E. C. M. Pennings, M. J. N. van Stralen, T. van Dongen, B. H. Verbeek, and J. M. M. van der Heijden, "Compact InP-based ring lasers employing multimode interference couplers and combiners," *Appl. Phys. Lett.*, vol. 64, no. 14, pp. 1753–1755, 1994.
[7] H. F. Talbot, "Facts relating to optical science No. IV," *London, Edinburgh Philosophical Mag., J. Sci.*, vol. 9, pp. 401–407, Dec. 1836.
[8] D. Marcuse, *Light Transmission Optics*. New York: Van Nostrand Reinhold, 1972.
[9] O. Bryngdahl, "Image formation using self-imaging techniques," *J. Opt. Soc. Amer.*, vol. 63, no. 4, pp. 416–419, 1973.
[10] R. Ulrich, "Image formation by phase coincidences in optical waveguides," *Optics Commun.*, vol. 13, no. 3, pp. 259–264, 1975.
[11] ——, "Light-propagation and imaging in planar optical waveguides," *Nouv. Rev. Optique*, vol. 6, no. 5, pp. 253–262, 1975.
[12] R. Ulrich and G. Ankele, "Self-imaging in homogeneous planar optical waveguides," *Appl. Phys. Lett.*, vol. 27, no. 6, pp. 337–339, 1975.
[13] D. C. Chang and E. F. Kuester, "A hybrid method for paraxial beam propagation in multimode optical waveguides," *Trans. Microwave Theory Tech.*, vol. MTT-29, no. 9, pp. 923–933, 1981.
[14] C. M. Weinert and N. Agrawal, "Three-dimensional simulation of multimode interference devices," in *Proc. Integr. Phot. Res. (IPRC)*, San Francisco, Feb. 1994, pp. 287–289
[15] R. M. Knox and P. P. Toulios, "Integrated circuits for the millimiter through optical frequency range," in *Proc. Symp. Submillimiter Waves*, J. Fox, Ed., New York, Mar./Apr. 1970, pp. 497–516.
[16] P. N. Robson and P. C. Kendall, Eds., *Rib Waveguide Theory by the Spectral Index Method*, Optoelectronic Series, Research Studies Press Ltd. New York: Wiley, 1990.
[17] N. S. Kapany and J. J. Burke, *Optical Waveguides*. New York: Academic, 1972.
[18] E. C. M. Pennings, R. J. Deri, A. Scherer, R. Bhat, T. R. Hayes, N. C. Andreadakis, M. K. Smit, and R. J. Hawkins, "Ultra-compact, low-loss directional coupler structures on InP for monolithic integration," in *Proc. Integr. Phot. Res. (IPRC)*, Monterey, CA, Apr. 1991, post-deadline paper PD2.
[19] ——, "Ultracompact, low-loss directional couplers on InP based on self-imaging by multimode interference," *Appl. Phys. Lett.*, vol. 59, no. 16, pp. 1926–1928, 1991.
[20] F. B. Veerman, P. J. Schalkwijk, E. C. M. Pennings, M. K. Smit, and B. H. Verbeek, "An optical passive 3-dB TMI coupler with reduced fabrication tolerance sensitivity," *J. Lightwave Technol.*, vol. 10, no. 3, pp. 306–311, 1992.
[21] J. E. Zucker, K. L. Jones, T. H. Chiu, B. Tell, and K. Brown-Goebeler, "Polarization-independent electro-optic waveguide switch using strained InGaAs/InP quantum wells," in *Proc. Integr. Phot. Research (IPRC)*, New Orleans, LA, Apr. 1992. pp. 21–24, paper Pd7.
[22] M. Bachmann, P. A. Besse, and H. Melchior, "General self-imaging properties in $N \times N$ multi-mode interference couplers including phase relations," *Appl. Opt.*, vol. 33, no. 17, pp. 3905–3911, 1994.
[23] T. Niemeier and R. Ulrich, "Quadrature outputs from fiber interferometer with 4 × 4 coupler," *Opt. Lett.*, vol. 11, no. 10, pp. 677–679, 1986.
[24] P. Roth, "Passive integrated optic mixer providing quadrature outputs," in *Proc. European Conf. Integrated Optics (ECIO)*, Paris, France, 1989, pp. 169–173.
[25] P. Roth and O. Parriaux, "Integrated optic interferometer with phase diversity," in *Proc. Conf. on Integrated Optics and Optical Communications*, Kobe, Japan, 1989, pp. 120–121.
[26] E. C. M. Pennings, R. J. Deri, R. Bhat, T. R. Hayes, and N. C. Andreadakis, "Ultra-compact integrated all-passive optical 90° hybrid using self-imaging," in *Proc. European Conf. Opt. Commun. (ECOC)*, Berlin, Germany, Oct. 1992, pp. 461–464, paper We B10.4.
[27] ——, "Ultracompact, all-passive optical 90°-hybrid on InP using self-imaging," *IEEE Photon. Technol. Lett.*, vol. 6, no. 5, pp. 701–703, 1993.
[28] E. C. M. Pennings, "Bends in optical ridge waveguides, modeling and applications," Ph.D. thesis, Delft Univ. of Technology, Delft, The Netherlands, 1990.
[29] L. B. Soldano, F. B. Veerman, M. K. Smit, B. H. Verbeek, A. H. Dubost, and E. C. M. Pennings, "Planar monomode optical couplers based on multi-mode interference," *J. Lightwave Technol.*, vol. 10, no. 12, pp. 1843–1850, 1992.
[30] L. B. Soldano, F. B. Veerman, M. K. Smit, B. H. Verbeek, and E. C. M. Pennings, "Multimode interference couplers," in *Proc. Integr. Phot. Research (IPRC)*, Monterey, CA, Apr. 1991, p. 13, paper TuD1.
[31] L. B. Soldano, F. B. Veerman, M. K. Smit, B. H. Verbeek, A. H. Dubost, and E. C. M. Pennings, "High-performance monomode planar couplers using a short multi-mode interference section," in *Proc. European Conf. Opt. Commun. (ECOC)*, Paris, France, Sept. 1991, pp. 225–228, paper TuB5-2.
[32] L. H. Spiekman, Y. S. Oei, E. G. Metaal, F. H. Groen, I. Moerman, and M. K. Smit, "Extremely small multimode interference couplers and ultrashort bends on InP by deep etching," *IEEE Photon. Technol. Lett.*, 1994, accepted for publication.
[33] R. M. Jenkins, R. W. J. Deveraux, and J. M. Heaton, "Waveguide beam splitters and recombiners based on multimode propagation phenomena," *Opt. Lett.*, vol. 17, no. 14, pp. 991–993, 1992.
[34] J. M. Heaton, R. M. Jenkins, D. R. Wight, J. T. Parker, J. C. H. Birbeck, and K. P. Hilton, "Novel 1-to-N way integrated optical beam splitters using symmetric mode mixing in GaAs/AlGaAs multimode waveguides," *Appl. Phys. Lett.*, vol. 61, no. 15, pp. 1754–1756, 1992.
[35] R. Ulrich and T. Kamiya, "Resolution of self-images in planar optical waveguides," *J. Opt. Soc. Amer.*, vol. 68, no. 5, pp. 583–592, 1978.
[36] L. B. Soldano, M. Bouda, M. K. Smit, and B. H. Verbeek, "New small-size single-mode optical power splitter based on multi-mode interference," in *Proc. European Conf. Opt. Commun. (ECOC)*, Berlin, Germany, Sept. 1992, pp. 465–468, paper We B10.5.
[37] T. P. Young, S. N. Radcliffe, A. J. Davies, and P. Smith, "Beamer—A design tool for integrated optics," *GEC J. Res.*, vol. 6, no. 3, pp. 152–161, 1988.
[38] C. Rolland, D. M. Adams, D. Yevick, and B. Hermansson, "Optimization of strongly guiding semiconductor rib waveguide Y-junctions," *IEEE Photon. Technol. Lett.*, vol. 2, no. 6, pp. 404–406, 1990.
[39] A. Ferreras, F. Rodríguez, E. Gómez-Salas, J. L. de Miguel, and F. Hernández-Gil, "Design and fabrication of a InP/InGaAsP multimode power splitter," in *Proc. Integr. Phot. Research (IPRC)*, Palm Springs, CA, Mar. 1993, pp. 151–154. paper IME4.
[40] ——, "Useful formulas for multimode interference power splitter/combiner design," *IEEE Photon. Technol. Lett.*, vol. 5, no. 10, pp. 1224–1227, 1993.
[41] L. B. Soldano, M. Bachmann, P. A. Besse, M. K. Smit, and H. Melchior, "Large optical bandwidth of InGaAsP/InP multi-mode interference 3-dB couplers," in *Proc. European Conf. Integrated Optics (ECIO)*, Neuchâtel, Switzerland, Apr. 1993, pp. 14.10–14.11.
[42] L. H. Spiekman, Y. S. Oei, E. G. Metaal, F. H. Groen, I. Moerman, M. K. Smit, and B. H. Verbeek, "Extremely small, fabrication-tolerant InP-based power-splitting and combining structures by deep etching," in *Proc. European Conf. Opt. Commun. (ECOC)*, Firenze, Italy, Sept. 1994, paper We.C.2.3.
[43] L. B. Soldano, A. H. de Vreede, M. K. Smit, B. H. Verbeek, E. G. Metaal, and F. H. Groen, "Mach-Zehnder interferometer polarization splitter in InGaAsP/InP," *IEEE Photon. Technol. Lett.*, vol. 6, no. 3, pp. 402–405, 1994.
[44] E. C. M. Pennings, R. van Roijen, M. J. N. van Stralen, P. J. de Waard, R. G. M. P. Koumans, and B. H. Verbeek, "Reflection properties of multimode interference devices," *IEEE Photon. Technol. Lett.*, vol. 6, no. 6, pp. 715–718, 1994.
[45] E. C. M. Pennings, R. van Roijen, M. J. N. van Stralen, B. H. Verbeek, J. M. M. van der Heijden, and T. van Dongen, "Spectral behavior of InP-based ring lasers employing multimode interference devices," in *Proc. Laser and Electro-Optics Society (LEOS)*, San José, CA, Nov. 1993, paper SCL10.1.
[46] P. A. Besse, M. Bachmann, H. Melchior, L. B. Soldano, and M. K. Smit, "Optical bandwidth and fabrication tolerances of multimode interference couplers," *J. Lightwave Technol.*, vol. 12, no. 6, pp. 1004–1009, 1994.
[47] J. C. Campbell and T. Li, "Electro-optic multimode waveguide switch," *Appl. Phys. Lett.*, vol. 33, no. 8, pp. 710–712, 1978.
[48] ——, "Electro-optic multimode waveguide modulator or switch," *J. Appl. Physics*, vol. 50, no. 10, pp. 6149–6154, 1979.
[49] R. J. Deri, E. C. M. Pennings, A. Scherer, A. S. Gozdz, C. Caneau, N. C. Andreadakis, V. Shah, L. Curtis, J. B. D. Soole, and J.-I. Song, "Ultra-compact, monolithic integration of balanced, polarization-diversity pho-

todetectors," in *Proc. European Conf. Opt. Commun. (ECOC)*, Berlin, Germany, Oct. 1992, pp. 457–460, paper We B10.3.
[50] R. J. Deri, R. Welter, E. C. M. Pennings, C. Caneau, J. L. Jackel, R. J. Hawkins, J. J. Johnson, H. Gilchrist, and C. Gibbons, "High-speed heterodyne operation of monolithically integrated balanced polarisation diversity photodetectors," *Electron. Lett.*, vol. 28, no. 25, pp. 2332–2334, 1992.
[51] E. C. M. Pennings, unpublished material, 1993.
[52] R. J. Deri, R. J. Hawkins, C. Caneau, E. C. M. Pennings, and N. C. Andreadakis, "Ultracompact monolithic integration of polarization diversity waveguide/photodiodes," *Appl. Phys. Lett.*, vol. 59, no. 15, pp. 1823–1825, 1991.
[53] N. Agrawal, D. Franke, C. M. Weinert, and C. Bornholdt, "2 × 2 optical space switches using InGaAsP/InP MQW structures for 10-GHz applications," in *Proc. Conf. Opt. Fiber Commun. (OFC)*, San Jośe, CA, Feb. 1994, pp. 148–149, paper WL7.
[54] R. M. Jenkins, R. W. J. Devereux, and J. M. Heaton, "A novel waveguide Mach-Zehnder interferometer based on multimode interference phenomena," *Optics Commun.*, vol. 109, pp. 410–424, Aug. 1994.
[55] P. A. Besse, M. Bachmann, and H. Melchior, "Phase relations in multi-mode interference couplers and their applications to generalized integrated Mach-Zehnder optical switches," in *Proc. European Conf. Integrated Optics (ECIO)*, Neuchâtel, Switzerland, Apr. 1993, pp. 2.22–2.23.
[56] R. M. Jenkins, J. M. Heaton, D. R. Wight, J. T. Parker, J. C. H. Birbeck, G. W. Smith, and K. P. Hilton, "Novel 1 × N and N × N integrated optical switches using self-imaging multimode GaAs/AlGaAs waveguides," *Appl. Phys. Lett.*, vol. 64, no. 6, pp. 684–686, 1994.
[57] M. Bachmann, C. Nadler, P. A. Besse, and H. Melchior, "Compect polarization-insensitive multi-leg 1 × 4 Mach-Zehnder switch in InGaAsP/InP," in *Proc. European Conf. Opt. Commun. (ECOC)*, Firenze, Italy, Sept. 1994, paper We.A.1.4.
[58] R. S. Burton, T. E. Schlesinger, and M. Munowitz, "An investigation of the modal coupling of simple branching semiconductor ring lasers," *J. Lightwave Technol.*, vol. 12, no. 5, pp. 754–759, 1994.
[59] T. Krauss, R. M. DeLaRue, I. Gontijo, P. J. R. Laybourn, and J. S. Roberts, "Strip-loaded semiconductor ring lasers employing multi-mode interference (MMI) output couplers," *Appl. Phys. Lett.*, 1994, submitted for publication.
[60] T. Krauss, R. M. DeLaRue, and P. J. R. Laybourn, "Impact of outcoupler configuration on operating characteristics of semiconductor ring lasers," submitted to *J. Lightwave Technol.*, 1994.
[61] J. M. Heaton, private communication, 1994.
[62] P. A. Besse, E. Gini, M. Bachmann, and H. Melchior, "New 1 × 2 multi-mode interference couplers with free selection of power splitting ratios," in *Proc. European Conf. Opt. Commun. (ECOC)*, Firenze, Italy, Sept. 1994, paper We.C.2.4.
[63] K. Al-hemyari, G. F. Doughty, C. D. W. Wilkinson, A. H. Kean, and C. R. Stanley, "Optical loss measurements on GaAs/GaAlAs single-mode waveguide Y-junctions and waveguide bends," *J. Lightwave Technol.*, vol. 11, no. 2, pp. 272–276, 1993.
[64] L. M. Caughan, N. Agrawal, and G. A. Bogert, "Novel physical effects in intersecting waveguides," *Appl. Phys. Lett.*, vol. 51, no. 18, pp. 1389–1391, 1987.
[65] R. Adar, C. H. Henry, R. F. Kazarinov, R. C. Kistler, and G. R. Weber, "Adiabatic 3-dB couplers, filters, and multiplexers made with silica waveguides on silicon," *J. Lightwave Technol.*, vol. 10, no. 1, pp. 46–50, 1992.
[66] C. Caldera, C. de Bernardi, G. Destefanis, M. Meliga, S. Morasca, and C. Rigo, "3-dB couplers integrated in InGaAlAs/InP for coherent applications," in *Proc. European Conf. Opt. Commun. (ECOC)*, Amsterdam, The Netherlands, Sept. 1990, pp. 357–360, paper TuP3.
[67] M. Zirngibl, C. Dragone, C. H. Joyner, M. Kouznetsov, and U. Koren, "Efficient 1 × 16 optical power splitter based on InP," *Electron. Lett.*, vol. 28, no. 13, pp. 1212–1213, 1992.
[68] C. Dragone, C. H. Henry, I. P. Kaminow, and R. C. Kistler, "Efficient multichannel integrated optics star coupler on silicon," *IEEE Photon. Technol. Lett.*, vol. 1, no. 8, pp. 241–243, 1989.
[69] K. Okamoto, H. Takahashi, M. Yasu, and Y. Hibino, "Fabrication of wavelength-insensitive 8 × 8 star coupler," *IEEE Photon. Technol. Lett.*, vol. 4, no. 1, pp. 61–63, 1992.

Lucas B. Soldano was born in Buenos Aires, Argentina, in 1960. He studied at Buenos Aires University, where he received the Electronics Engineer degree in 1988. During his studies he was active in the field of gas- and solid-state lasers. He received the Design Engineer degree in microelectronics in 1991, and the Ph.D. degree in integrated optics in 1994, both from Delft University of Technology, Delft, the Netherlands. His thesis research was on passive integrated optical devices based on multimode interference.

Recently, he joined the Centro Studi e Laboratori Telecomunicazioni, Turin, Italy, where he is engaged in research on integrated-optic devices and rare-earth doped waveguides.

Erik C. M. Pennings (S'88–M'90) was born in Sassenheim, The Netherlands, on November 3, 1960. He received the M.Sc. degree (cum laude) in applied physics from Groningen University, in 1986, and the Ph.D. degree in electrical engineering from Delft University of Technology, The Netherlands, in 1990. His thesis describes modeling and experiments on bends in optical waveguides and on multimode interference couplers.

He subsequently joined Bell Communications Research in Red Bank, NJ, as a post-doctoral member of technical staff, where he worked on InP-based photonic integrated circuits, more specifically on curved waveguides, multimode interference devices, photodiodes, and application of these components in an optical polarization-diversity coherent reeiver chip. In 1992, he joined the group Wideband Communication Systems of Philips Research Laboratories, Eindhoven, The Netherlands. His current research interests include polarization controllers, microoptical and fiber-based components for high-bitrate optical communication systems, and semiconductor ring lasers. He has written and coauthored over 45 scientific papers and conference contributions.

Dr. Pennings is a member of the Dutch Physical Society (NNV) and the OSA.